

Observation of Spin-orbit Magnetoresistance in CoFeB/HM/MgO with existence of both spin Hall effect and Edelstein effect

Haoran Ni, Shuangfeng Li, Qihan Zhang, Xiaolong Fan*

*Key Laboratory for Magnetism and Magnetic Materials of the Ministry of Education
Lanzhou University, Lanzhou, 730000, People's Republic of China*

Corresponding author: Xiaolong Fan

E-mail address: fanxiaolong@lzu.edu.cn

Abstract

In this paper, we report the observation of spin-orbit magnetoresistance (SOMR) in Ferromagnetic Metal/Heavy Metal/MgO system. We measure the magnetoresistance as the function of the thickness of Heavy Metal (HM) for CoFeB/HM/MgO and CoFeB/HM films where HM = Pt and Ta. The evidence of the SOMR is indicated by a peak of the MR ratio when the thickness of HM is around $1 \sim 2$ nm for CoFeB/HM/MgO films, which is absent for CoFeB/HM films. We speculate the SOMR observed in our experiment originates from the spin-orbit coupling at the HM/MgO interface. We give the boundary conditions of our samples and calculate the theoretical magnetoresistance based on spin diffusion equation. Following the function we get, we can explain the two peaks we observe separately comes from the spin Hall effect and Edelstein effect.

Introduction

Magnetoresistance (MR) effect has long been studied, and their tunable property may provide potential application for future memory devices. In recent years, there have been a lot of reports about new unconventional magnetoresistances. The Spin Hall Magnetoresistance (SMR), which is the result of the interaction between Spin Hall Effect (SHE) and Inverse Spin Hall Effect (ISHE) [1], depends on the angle between magnetization and spin polarization, and it has been reported in several heterostructure systems[2,3]; The recently reported Hanle Magnetoresistance (HMR)

depends on the direction and strength of external magnetic field, and it appears in thin metal film which has a strong spin-orbit coupling [4,5]; The Rashba-Edelstein Magnetoresistance (REMR) is reported in Bi/Ag/CoFeB trilayer, and this magnetoresistance is the result of interfacial spin-orbit coupling and spin-current reflection in the metallic heterostructure [6]. Those unconventional MR effect can help us understand the spin-charge conversion by either bulk or interfacial effect better.

Recently, a new type of magnetoresistance was predicted [7], called spin-orbit magnetoresistance (SOMR). It originates from the Rashba type spin-orbit coupling at the interface. Its angular dependence on M is identical to SMR. Though having identical angular dependence, it is proposed that we can differentiate SOMR from SMR by their thickness dependence.

The first experimental observation of SOMR was done by Lifan Zhou *et al.* They observed SOMR in Cu[Pt]/YIG structure [8]. They confirmed that SOMR does have different thickness dependence from SMR. SOMR brings out another peak other than the conventional SMR peak, and that peak appears when the thickness of HM is very thin, because the Rashba spin-orbit coupling is enhanced by the scattered heavy metal islands according to their explanation.

In our experiments, we conduct MR measurements on CoFeB/Ta/MgO and CoFeB/Pt/MgO samples and observe the same SOMR phenomenon at thin HM layer. We then do MR measurements on CoFeB/Ta and CoFeB/Pt to confirm the MR we observe is SOMR and that it originates from the HM/MgO interface. Instead of using the theory proposed in paper[7], we would like to use the conventional spin diffusion equation to explain our result, because our samples are slightly different from that of Lifan Zhou's group. Besides the conventional boundary condition at FM/HM interface, we give the boundary condition of our samples at HM/MgO interface, and solve the spin diffusion equation. The function we get has four parts, two of them coming from the spin current induced by spin Hall effect, another two coming from the spin current induced by Edelstein effect, and the two group corresponds to the two peaks in our experiment separately. The validity of our result can also be confirmed by ignoring the SHE and ISHE part in our function, which brings us back to the result of pure Edelstein effect[26].

Fabrications

We fabricated six sets of samples: (i) CoFeB(5 nm)/Ta(d_{Ta})/MgO(3 nm); (ii) CoFeB(5 nm)/Ta(d_{Ta}); (iii) CoFeB(5 nm)/Pt(d_{Pt})/MgO(3 nm); (iv) CoFeB(5 nm)/Pt(d_{Pt}); (v) CoFeB(d_{CoFeB})/Ta(10 nm)/MgO(3 nm); (vi) CoFeB(d_{CoFeB})/Pt(10 nm)/MgO(3 nm). All of them were fabricated on Si (100) substrates using magnetron sputtering under room temperature, the background pressure of which was controlled to be 2×10^{-7} Torr, and the pressure of Argon gas was controlled to be 5 mTorr.

Experimental results

The thickness of the layers are determined by X-ray reflectivity (XRR), a typical data for CoFeB(5 nm)/Pt(10 nm) is shown in FIG. 1[a]. From the number and the intensity of the peaks we can determine the thickness and roughness of our samples.

We perform angular-dependent MR measurements in two planes, one is called β and one is called γ , which are shown in FIG. 1[b]. The definition of the angles is shown in the picture, and the external magnetic field is controlled to be ~ 1.35 T. Because those two directions are both out-of-plane directions, the saturated magnetic field under that circumstance will be very high, therefore the original SMR plots we get are not ideal sinusoidal curves. In order to get the conventional sinusoidal curve, the misalignment of \mathbf{H} and \mathbf{M} has to be considered. We use the equation derived from static equilibrium condition of magnetization:

$$2H \sin(\beta - \beta_M) + \mu_0 M_{eff} \sin(2\beta_M) = 0 \quad (1)$$

to determine the angle of \mathbf{M} , where $\mu_0 M_{eff}$ is the effective demagnetization field which is determined using Magneto-optical Kerr effect.

A typical data for Magneto-optical Kerr effect is shown in FIG. 1[c], and the sample used here is CoFeB(5 nm)/Ta(1.5 nm)/MgO(3 nm). The magnetic field is applied perpendicular to the surface of the sample to measure its Kerr signal as a function of external magnetic field. From FIG. 1[c] we can see that there is no magnetic hysteresis in this system, which implies there is no vertical magnetic anisotropy in this sample, and it is saturated under a magnetic field higher than 1.3 T, therefore we can safely take the saturated magnetic field as the demagnetization field.

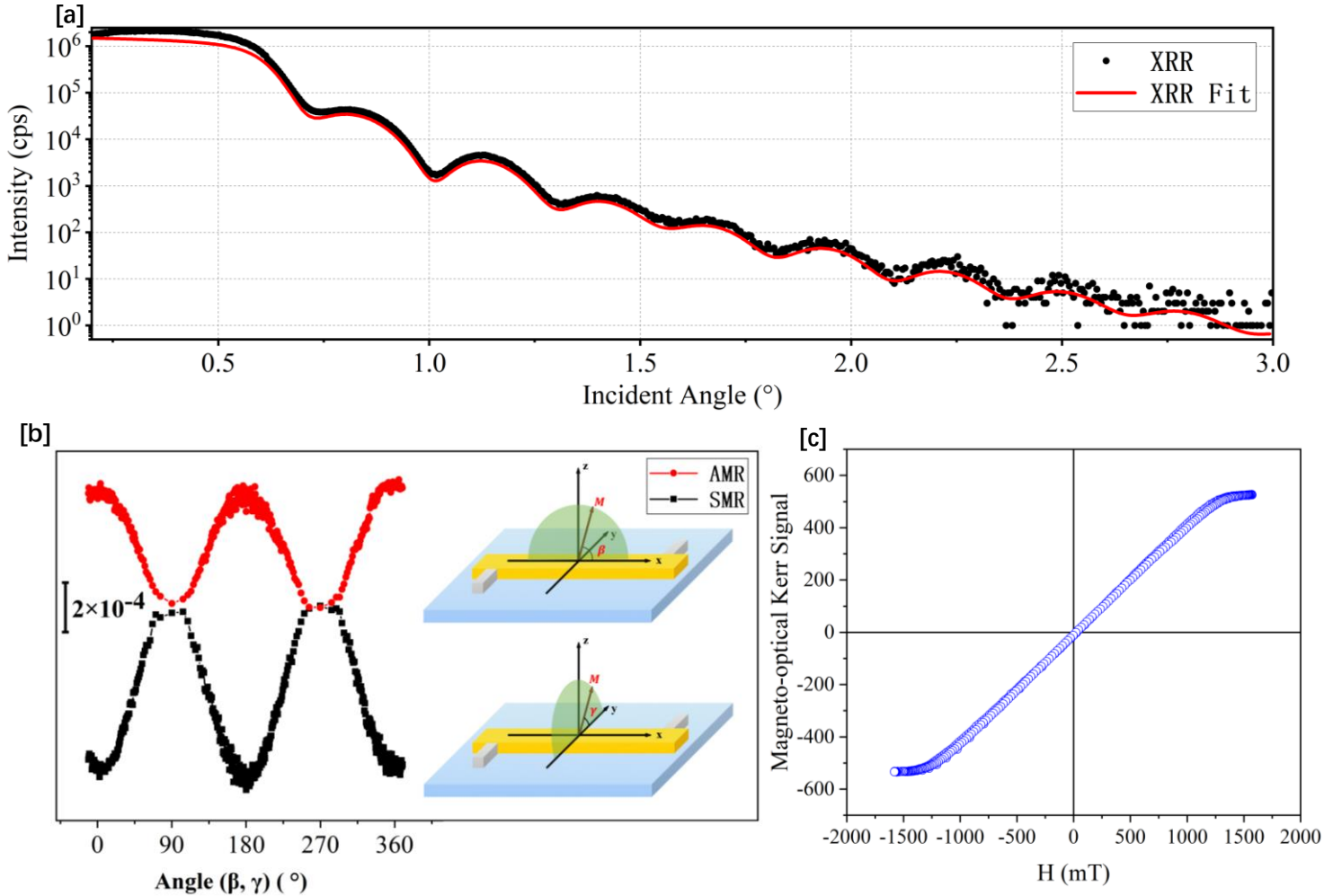


FIG. 1. [a] XRR measurements. [b] MR measurements set up. The black line (SMR) corresponds to γ measurement, and the red line (AMR) corresponds to β measurement. [c] Magneto-optical Kerr effect measurement (300K).

We observe both SMR and AMR in our MR measurements. SMR looks quite similar to AMR, but their dependence on angle differ, which provides a way to distinguish them. AMR depends on the angle between magnetization and charge current, while SMR depends on the angle between magnetization and spin polarization, namely the angle between the external field and spin polarization. And the reason why we did not perform a MR measurement in x - y plane is that, SMR and AMR will mix in x - y plane measurements, making it difficult to analyze the SMR effect that we are focusing on. In β measurements, only the angle between external field and charge current is changing, therefore the MR can only originate from AMR. In γ measurements, only the angle between external field and spin polarization is changing, therefore the MR can only originate from SMR. The difference of these two effects is shown in FIG. 1[b]. We will focus on γ measurements.

In the paper of Lifan Zhou *et al.*'s work[8], they discovered that SOMR appears as another peak before the peak of SMR. We observe the same effect in our measurements. See FIG. 2 [c]. When the HM layer is thin, the MR effect is very small. As the thickness increases, 2nm for CoFeB(10 nm)/Ta(d_{Ta})/MgO(3 nm) and 1.25nm for CoFeB(10 nm)/Pt(d_{Pt})/MgO(3 nm), the MR effect reaches a maximum, which is the SOMR effect we observe. Then it decreases for Ta = 3nm and Pt = 2nm. The MR effect reaches a maximum again for Ta = 5nm and Pt = 2.5nm, which is the sign of the conventional SMR effect. When Ta is thicker than 5nm and Pt is thicker than 2.5nm, the MR effect decreases again. The change of MR ratio as the function of HM thickness is shown in FIG. 2[a] and FIG. 2[b].

In order to make sure that the MR we observe is SOMR and that it is generated at the interface between HM(Pt, Ta) and MgO, we did exact the same measurements on CoFeB(10 nm)/Ta(d_{Ta}) and CoFeB(10 nm)/Pt(d_{Pt}). The $\Delta\rho/\rho$ diagrams of those two series are shown in FIG. 2[a] and FIG. 2[b]. As we expected, the SOMR peak disappears in this case. This result confirms that the MR we observe is SOMR and it originates from the interface between the metal layer and MgO layer.

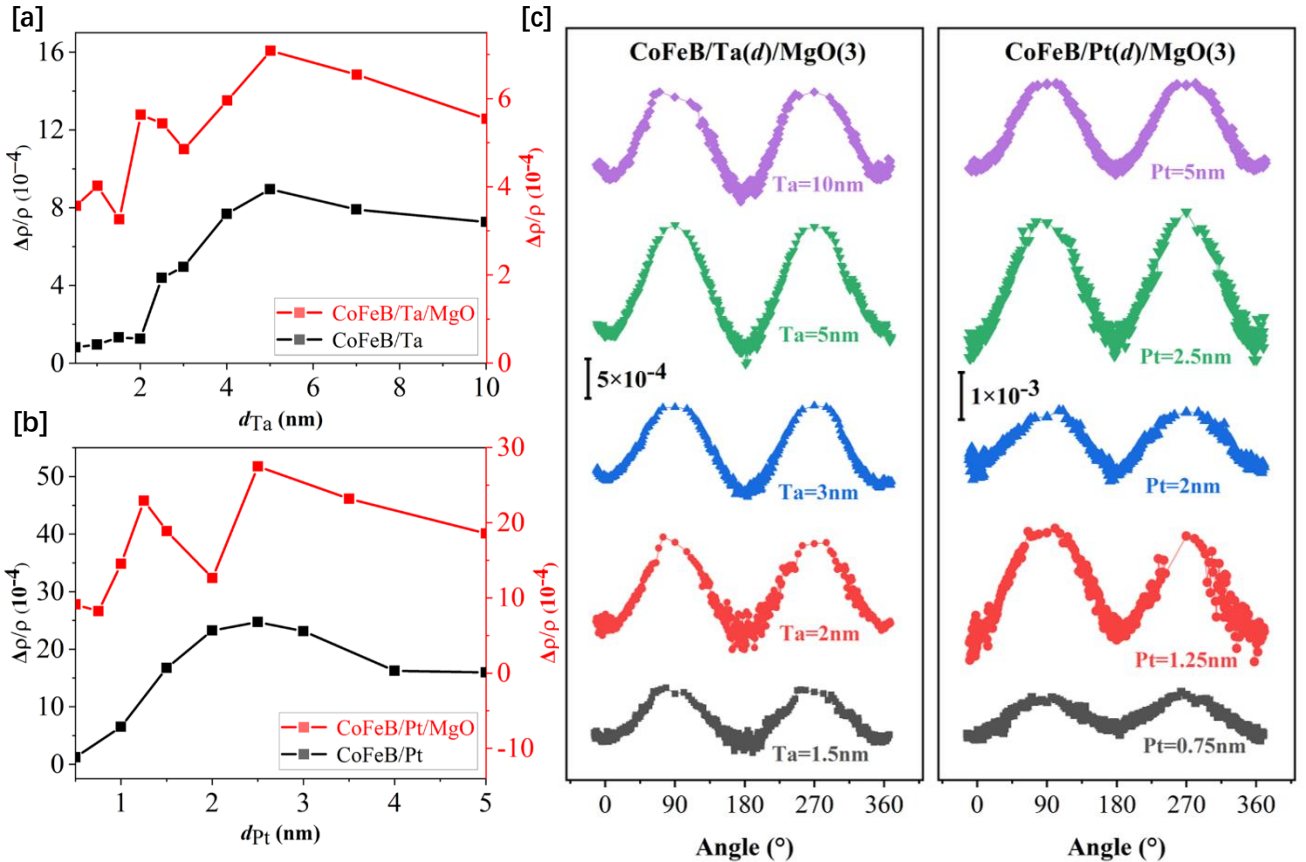


FIG. 2. [a] Ta layer thickness dependence of MR ratio for CoFeB(5 nm)/Ta(d_{Ta})/MgO(3 nm) and CoFeB(5 nm)/Ta(d_{Ta}) respectively. [b] Pt layer thickness dependence of MR ratio for CoFeB(5 nm)/Pt(d_{Pt})/MgO(3 nm) and CoFeB(5 nm)/Pt(d_{Pt}) respectively. [c] Angular dependent MR measurements in γ direction for CoFeB(5 nm)/Ta(d_{Ta})/MgO(3 nm) and CoFeB(5 nm)/Pt(d_{Pt})/MgO(3 nm).

Analysis



FIG. 3. Notations

In our samples, there are two main effects that generate spin current, spin Hall effect in HM layer and Edelstein effect at HM/MgO interface. We give the boundary conditions:

$$z = 0: \quad e\mathbf{j}_s^z(z = 0) = G_r \hat{\mathbf{m}} \times [\hat{\mathbf{m}} \times \boldsymbol{\mu}_s(0)] + G_i \hat{\mathbf{m}} \times \boldsymbol{\mu}_s(0) \quad (2)$$

$$z = d: \quad \boldsymbol{\mu}_s(d) = (\mu_s^R - \mu_s^0) \hat{\mathbf{y}} \quad (3)$$

where $G_{\uparrow\downarrow} = G_r + iG_i$ is the spin-mixing conductance; $\boldsymbol{\mu}_s(z)$ is the spin accumulation; $\mu_s^R = \eta \frac{3m_e^*}{2e\hbar\epsilon_F} \frac{1}{D(\epsilon_F)} \alpha_{R_eff} j_c^0$, where α_{R_eff} is the Rashba parameter, $D(\epsilon_F)$ is the density of states; $\mu_s^0 = \frac{2e\lambda}{\sigma} \tanh \frac{d}{2\lambda} j_{s0}^{SH}$, where λ is the spin diffusion length, $j_{s0}^{SH} = \theta_{SH} j_c^0$ is the spin current caused by spin Hall effect, θ_{SH} is the spin Hall angle.

The overall spin current in our sample can be written as:

$$\mathbf{j}_s^z(z) = -\frac{\sigma}{2e} \partial_z \boldsymbol{\mu}_s - j_{s0}^{SH} \hat{\mathbf{y}} \quad (4)$$

Using spin diffusion equation, we get

$$\boldsymbol{\mu}_s(z) = \mu_s^R \hat{\mathbf{y}} \frac{\cosh \frac{z}{\lambda}}{\cosh \frac{d}{\lambda}} + \mu_s^0 \hat{\mathbf{y}} \frac{\sinh \frac{d-2z}{2\lambda}}{\sinh \frac{d}{2\lambda}} + \frac{2e\lambda}{\sigma} \frac{\sinh \frac{d-z}{\lambda}}{\cosh \frac{d}{\lambda}} \mathbf{j}_s^z(0) \quad (5)$$

Solve $\mathbf{j}_s^z(0)$ to obtain

$$\begin{aligned}
\mu_s(z) = & \mu_s^R \hat{\mathbf{y}} \frac{\cosh \frac{z}{\lambda}}{\cosh \frac{d}{\lambda}} + \frac{2\lambda}{\sigma} \mu_s^R \hat{\mathbf{m}} \times (\hat{\mathbf{m}} \times \hat{\mathbf{y}}) Re \frac{G_{\uparrow\downarrow}}{1 + \frac{2\lambda}{\sigma} G_{\uparrow\downarrow} \tanh \frac{d}{\lambda}} \frac{\sinh \frac{d-z}{\lambda}}{\cosh^2 \frac{d}{\lambda}} \\
& + \frac{2\lambda}{\sigma} \mu_s^R \hat{\mathbf{m}} \times \hat{\mathbf{y}} Im \frac{G_{\uparrow\downarrow}}{1 + \frac{2\lambda}{\sigma} G_{\uparrow\downarrow} \tanh \frac{d}{\lambda}} \frac{\sinh \frac{d-z}{\lambda}}{\cosh^2 \frac{d}{\lambda}} + \mu_s^0 \hat{\mathbf{y}} \frac{\sinh \frac{d-2z}{2\lambda}}{\sinh \frac{d}{\lambda}} \\
& + \frac{2\lambda}{\sigma} \mu_s^0 \hat{\mathbf{m}} \times (\hat{\mathbf{m}} \times \hat{\mathbf{y}}) Re \frac{G_{\uparrow\downarrow}}{1 + \frac{2\lambda}{\sigma} G_{\uparrow\downarrow} \tanh \frac{d}{\lambda}} \frac{\sinh \frac{d-z}{\lambda}}{\cosh \frac{d}{\lambda}} \\
& + \frac{2\lambda}{\sigma} \mu_s^0 \hat{\mathbf{m}} \times \hat{\mathbf{y}} Im \frac{G_{\uparrow\downarrow}}{1 + \frac{2\lambda}{\sigma} G_{\uparrow\downarrow} \tanh \frac{d}{\lambda}} \frac{\sinh \frac{d-z}{\lambda}}{\cosh \frac{d}{\lambda}}
\end{aligned} \tag{6}$$

The first three items of the above function are exactly the same as the $\mu_s(z)$ given in [26], and the left two items characterize the affect brought by spin Hall effect.

$$\begin{aligned}
j_s^z(z) = & -\frac{\sigma}{2e\lambda} \mu_s^R \hat{\mathbf{y}} \frac{\sinh \frac{z}{\lambda}}{\cosh \frac{d}{\lambda}} + \frac{1}{e} \mu_s^R \hat{\mathbf{m}} \times (\hat{\mathbf{m}} \times \hat{\mathbf{y}}) Re \frac{G_{\uparrow\downarrow}}{1 + \frac{2\lambda}{\sigma} G_{\uparrow\downarrow} \tanh \frac{d}{\lambda}} \frac{\cosh \frac{d-z}{\lambda}}{\cosh^2 \frac{d}{\lambda}} \\
& + \frac{1}{e} \mu_s^R \hat{\mathbf{m}} \times \hat{\mathbf{y}} Im \frac{G_{\uparrow\downarrow}}{1 + \frac{2\lambda}{\sigma} G_{\uparrow\downarrow} \tanh \frac{d}{\lambda}} \frac{\cosh \frac{d-z}{\lambda}}{\cosh^2 \frac{d}{\lambda}} + \frac{\sigma}{2e\lambda} \mu_s^0 \hat{\mathbf{y}} \frac{\cosh \frac{d-2z}{2\lambda}}{\sinh \frac{d}{2\lambda}} \\
& + \frac{1}{e} \mu_s^0 \hat{\mathbf{m}} \times (\hat{\mathbf{m}} \times \hat{\mathbf{y}}) Re \frac{G_{\uparrow\downarrow}}{1 + \frac{2\lambda}{\sigma} G_{\uparrow\downarrow} \tanh \frac{d}{\lambda}} \frac{\cosh \frac{d-z}{\lambda}}{\cosh \frac{d}{\lambda}} \\
& + \frac{1}{e} \mu_s^0 \hat{\mathbf{m}} \times \hat{\mathbf{y}} Im \frac{G_{\uparrow\downarrow}}{1 + \frac{2\lambda}{\sigma} G_{\uparrow\downarrow} \tanh \frac{d}{\lambda}} \frac{\cosh \frac{d-z}{\lambda}}{\cosh \frac{d}{\lambda}} - j_{s0}^{SH} \hat{\mathbf{y}}
\end{aligned} \tag{7}$$

Knowing $j_s^z(z)$, we can obtain the current in $\hat{\mathbf{x}}$ direction $(j_{cx})_s$

$$\begin{aligned}
(j_{cx})_s = & j_c^0 - \frac{\theta_{SH}\sigma}{2e\lambda} \mu_s^R \frac{\sinh \frac{z}{\lambda}}{\cosh \frac{d}{\lambda}} + \frac{\theta_{SH}}{e} \mu_s^R (m_y^2 - 1) Re \frac{G_{\uparrow\downarrow}}{1 + \frac{2\lambda}{\sigma} G_{\uparrow\downarrow} \tanh \frac{d}{\lambda}} \frac{\cosh \frac{d-z}{\lambda}}{\cosh^2 \frac{d}{\lambda}} \\
& + \frac{\theta_{SH}\sigma}{2e\lambda} \mu_s^0 \frac{\cosh \frac{d-2z}{2\lambda}}{\sinh \frac{d}{2\lambda}} + \frac{\theta_{SH}}{e} \mu_s^0 (m_y^2 - 1) Re \frac{G_{\uparrow\downarrow}}{1 + \frac{2\lambda}{\sigma} G_{\uparrow\downarrow} \tanh \frac{d}{\lambda}} \frac{\cosh \frac{d-z}{\lambda}}{\cosh \frac{d}{\lambda}}
\end{aligned}$$

The Inverse Edelstein effect at HM/MgO interface also contributes to the charge current in $\hat{\mathbf{x}}$ direction

$$\begin{aligned}
(\delta j_c)_x = & \lambda_{IEE} [\mathbf{j}_s^z(d) \times \hat{\mathbf{z}}]_x \\
= & -\frac{\lambda_{IEE}\sigma}{2e\lambda} \mu_s^R \frac{\sinh \frac{d}{\lambda}}{\cosh \frac{d}{\lambda}} + \frac{\lambda_{IEE}}{e} \frac{\mu_s^R}{\cosh^2 \frac{d}{\lambda}} (m_y^2 - 1) Re \frac{G_{\uparrow\downarrow}}{1 + \frac{2\lambda}{\sigma} G_{\uparrow\downarrow} \tanh \frac{d}{\lambda}} + \frac{\lambda_{IEE}\sigma}{2e\lambda} \mu_s^0 \frac{\cosh \frac{d}{2\lambda}}{\sinh \frac{d}{2\lambda}} \\
& + \frac{\lambda_{IEE}}{e} \frac{\mu_s^0}{\cosh \frac{d}{\lambda}} (m_y^2 - 1) Re \frac{G_{\uparrow\downarrow}}{1 + \frac{2\lambda}{\sigma} G_{\uparrow\downarrow} \tanh \frac{d}{\lambda}} - \lambda_{IEE} j_{s0}^{SH}
\end{aligned} \tag{8}$$

Therefore we have

$$j_{cx} = (j_{cx})_s + (\delta j_c)_x \quad (9)$$

$$\rho = \rho_0 + \Delta\rho_1 + \Delta\rho_2(1 - m_y^2) \quad (10)$$

where

$$\begin{aligned} \frac{\Delta\rho_2}{\rho_0} = \zeta^2 \left[\frac{\theta_{SH}}{e} \xi_{EE} \frac{\lambda \tanh \frac{d}{\lambda}}{d \cosh \frac{d}{\lambda}} + \frac{\lambda_{IEE}}{e} \frac{\xi_{EE}}{\cos^2 \frac{d}{\lambda}} + 2\lambda\theta_{SH}^2 \frac{\lambda}{d} \tanh \frac{d}{\lambda} \tanh \frac{d}{2\lambda} \right. \\ \left. + 2\lambda\theta_{SH}\lambda_{IEE} \frac{\tanh \frac{d}{2\lambda}}{\cosh \frac{d}{\lambda}} \right] \frac{G_r}{\sigma + 2\lambda G_r \tanh \frac{d}{\lambda}} \end{aligned} \quad (11)$$

within which we let $\mu_s^R = E_x \xi_{EE}$, $G_r \gg G_i$, and consider the current shunting factor

$$\zeta = \frac{1}{1 + \frac{\rho_{HM}d_{FM}}{\rho_{FM}d_{HM}}} \frac{1}{1 + \frac{\rho_I d_{HM}}{\rho_{HM}d_I}} \quad (12)$$

where the subscript “I” stands for “Interface”. We draw the separate plot of each item in the above function

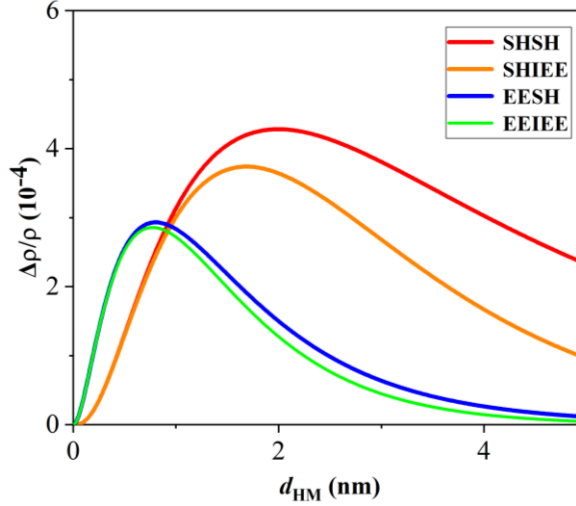


FIG. 4. The plots of each item in equation (11). The parameters are chosen to be $\theta_{SH} = 0.08$, $\lambda_{IEE} = 0.08$, $\xi_{EE}/e = 0.08 \text{ nm}$, $\lambda = 2 \text{ nm}$, $G_r = 9 \times 10^{15} \Omega^{-1} \text{ m}^{-2}$, $\sigma = 1 \times 10^7 \Omega^{-1} \text{ m}^{-1}$, $\rho_{HM}d_{FM}/\rho_{FM} = 1 \text{ nm}$, $\rho_I/(\rho_{HM}d_I) = 4 \text{ nm}$.

We can see that the spin current generated by Edelstein effect converts to charge current through Inverse spin Hall effect and Inverse Edelstein effect, and the magnetoresistance of those two reaches a maximum at very close HM thickness. The same is true for the spin current generated by spin Hall effect, which converts to charge current through Inverse spin Hall effect and Inverse Edelstein effect.

Therefore we can explain the two peaks in our experiment in this way. The first and smaller peak comes from the spin current generated by Edelstein effect and the second peak comes from the spin Hall effect. The relative magnitude of those two peaks characterize the relative “amount” of spin current generated by Edelstein effect and spin Hall effect.

However, our function fails to explain the two peak phenomenon when we add the four items together. Our experiment result, as well as that in [8], is too sharp to fit. The peak function given by solving spin diffusion equation is too smooth that when we add functions with different peak position together, the difference of peaks cancels out and only gives one peak. Some more precise theories are needed.

Conclusions

We report the SOMR effect in CoFeB/Ta/MgO and CoFeB/Pt/MgO system, and confirm that SOMR originates from the interface between HM and MgO. We propose the boundary condition at HM/MgO interface and solve the spin diffusion equation, and we use the function we get to explain the origin of the two peaks we observe. Our theory analysis is not satisfactory for the fact that our function cannot fit the data. Therefore we hope that some more accurate theory can be proposed to figure out the mechanism when spin Hall effect and Edelstein effect both exist.

References

- [1] Chen Y T, Takahashi S, Nakayama H, et al. Theory of spin Hall magnetoresistance[J]. Physical Review B, **2013**, 87(14): 144411.
- [2] Nakayama H, Althammer M, Chen Y T, et al. Spin Hall magnetoresistance induced by a nonequilibrium proximity effect[J]. Physical review letters, **2013**, 110(20): 206601.
- [3] Kim J, Sheng P, Takahashi S, et al. Spin Hall magnetoresistance in metallic bilayers[J]. Physical review letters, **2016**, 116(9): 097201.
- [4] Vélez S, Golovach V N, Bedoya-Pinto A, et al. Hanle magnetoresistance in thin metal films with strong spin-orbit coupling[J]. Physical review letters, **2016**, 116(1): 016603.
- [5] Wu H, Zhang X, Wan C H, et al. Hanle magnetoresistance: The role of edge spin accumulation

and interfacial spin current[J]. *Physical Review B*, **2016**, 94(17): 174407.

[6] Nakayama H, Kanno Y, An H, et al. Rashba-Edelstein magnetoresistance in metallic heterostructures[J]. *Physical review letters*, **2016**, 117(11): 116602.

[7] Grigoryan V L, Guo W, Bauer G E W, et al. Intrinsic magnetoresistance in metal films on ferromagnetic insulators[J]. *Physical Review B*, **2014**, 90(16): 161412.

[8] Zhou L, Song H, Liu K, et al. Observation of spin-orbit magnetoresistance in metallic thin films on magnetic insulators[J]. *Science advances*, **2018**, 4(1): eaao3318.

[9] Hirsch J E. Spin hall effect[J]. *Physical Review Letters*, **1999**, 83(9): 1834.

[10] Kato Y K, Myers R C, Gossard A C, et al. Observation of the spin Hall effect in semiconductors[J]. *science*, **2004**, 306(5703): 1910-1913.

[11] McGuire T, Potter R L. Anisotropic magnetoresistance in ferromagnetic 3d alloys[J]. *IEEE Transactions on Magnetics*, **1975**, 11(4): 1018-1038.

[12] Zhou L, Grigoryan V L, Maekawa S, et al. Spin Hall effect by surface roughness[J]. *Physical Review B*, **2015**, 91(4): 045407.

[13] Qin Z, Wang Y, Zhu S, et al. Stabilization and Reversal of Skyrmion Lattice in Ta/CoFeB/MgO Multilayers[J]. *ACS applied materials & interfaces*, **2018**, 10(42): 36556-36563.

[14] Fuchs K. The conductivity of thin metallic films according to the electron theory of metals[C]//*Mathematical Proceedings of the Cambridge Philosophical Society*. Cambridge University Press, **1938**, 34(1): 100-108.

[15] Takahashi S, Maekawa S. Spin current, spin accumulation and spin Hall effect[J]. *Science and Technology of Advanced Materials*, **2008**, 9(1): 014105.

[16] Qin Z, Wang Y, Zhu S, et al. Stabilization and Reversal of Skyrmion Lattice in Ta/CoFeB/MgO Multilayers[J]. *ACS applied materials & interfaces*, **2018**, 10(42): 36556-36563.

[17] Sondheimer E H. The mean free path of electrons in metals[J]. *Advances in Physics*, **2001**, 50(6): 499-537.

[18] Zhang W, Brongersma S H, Richard O, et al. Influence of the electron mean free path on the resistivity of thin metal films[J]. *Microelectronic Engineering*, **2004**, 76(1-4): 146-152.

[19] Zhou H, Fan X, Ma L, et al. Spatial symmetry of spin pumping and inverse spin Hall effect in the Pt/Y₃Fe₅O₁₂ system[J]. *Physical Review B*, **2016**, 94(13): 134421.

[20] Mayadas A F, Shatzkes M. Electrical-resistivity model for polycrystalline films: the case of

arbitrary reflection at external surfaces[J]. *Physical review B*, **1970**, 1(4): 1382.

[21] Namba Y. Resistivity and temperature coefficient of thin metal films with rough surface[J]. *Japanese Journal of Applied Physics*, **1970**, 9(11): 1326.

[22] Leontiadou M A, Litvinenko K L, Gilbertson A M, et al. Experimental determination of the Rashba coefficient in InSb/InAlSb quantum wells at zero magnetic field and elevated temperatures[J]. *Journal of Physics: Condensed Matter*, **2011**, 23(3): 035801.

[23] Eldridge P S, Leyland W J H, Lagoudakis P G, et al. Optical Measurement Of The Rashba Coefficient In GaAs/AlGaAs Quantum Wells[C]//AIP Conference Proceedings. AIP, **2010**, 1199(1): 395-396.

[24] Borge J, Gorini C, Vignale G, et al. Spin Hall and Edelstein effects in metallic films: From two to three dimensions[J]. *Physical Review B*, **2014**, 89(24): 245443.

[25] Manchon A, Koo H C, Nitta J, et al. New perspectives for Rashba spin–orbit coupling[J]. *Nature materials*, **2015**, 14(9): 871.

[26] Kim J , Chen Y T , Karube S , et al. Evaluation of bulk-interface contributions to Edelstein magnetoresistance at metal/oxide interfaces[J]. *Physical Review B*, **2017**, 96(14):140409.